Proceedings of the 25th International Conference on
Port and Ocean Engineering under Arctic Conditions
June 9-13, 2019, Delft, The Netherlands

Simulation of a ship advancing in floating ice floes

Luofeng Huang[1, *], Minghao Li[2], Bojan Igrec[1], Philip Cardiff[3],
Dimitris Stagonas[1,4], Giles Thomas[1]

[1] University College London, London, United Kingdom
[2] Chalmers University of Technology, Gothenburg, Sweden
[3] University College Dublin, Dublin, Ireland
[4]Cranfield University, Cranfield, United Kingdom

ABSTRACT

The effect of global warming is inducing sea ice retreat and transforming the Arctic into a navigable ocean. The melted ice cover can result in an environment where pancake-shaped ice floes are floating on sea surface; however, the effect of such an ice condition on ship performance has yet to be understood. This work develops a numerical model to predict the ship resistance in this typical case. Building on a traditional computational model for predicting ship hydrodynamics in open ocean, the Discrete Element Method is incorporated to include ice floes, so as to achieve ship-wave-ice coupling; thus, the simulation innovatively considers the influence of fluid flow on the interaction process. Following validation against experiments, the proposed model has been shown capable of accurately predicting ship resistance in pancake ice condition. Subsequently, the relationship of the resistance with ship speed, ice concentration and floe size is investigated.

KEY WORDS: Ship; Ice Floe; Computational Fluid Dynamics; Discrete Element Method.

INTRODUCTION

The effect of global warming is causing the sea ice extent in the Arctic to reduce quickly. Satellite images have observed its summer minimum to have decreased by approximately 12% per decade (Stroeve et al., 2012). The ice retreat creates open water and leads to the notion that commercial shipping routes through the Arctic region will become navigable (Smith and Stephenson, 2013). There are two main shipping routes through the Arctic: the Northwest Passage, which passes over the top of Canada and the United States; and the North Sea Route, which passes north of Norway and Russia. Both routes are shown in Figure 1, alongside the contemporary routes passing through the Suez and Panama Canals. Compared to the contemporary counterparts, the Arctic shipping routes are around 40% shorter in distance, which signifies considerable savings of time, fuel and emissions (Ørts Hansen et al., 2016). In addition to the major routes, there are also numerous routes opened for travels between

*Presenting Author: ucemlhu@ucl.ac.uk

continents and the Arctic, which are used to access abundant oil, gas, mines, fishing grounds and tourism.

While new shipping routes offering great opportunities, challenges arise since the potential navigation environment has been found to be more complex than anticipated. Rather than providing pure open water, the melting process of sea ice results in that the ice coverage breaks up into numerous ice floes floating on the sea surface, as shown in Figure 2. The shape of ice floes tends to be circular due to the effect of wave wash and floe–floe collisions, thus known as pancake ice. Field measurements and aerial observations have reported that such a pancake-ice environment will be the most ubiquitous environment of future Arctic (Parmiggiani et al., 2018; Thomson et al., 2018), which also dominates the new shipping routes; this means it is of great importance to study the effect of pancake ice on ship performance; however, such effect has yet to be well understood.

The presence of numerous ice floes results in the problem being highly complex, and only a small number of experiments have attempted to replicate the process. Guo et al. (2018) measured the resistance of an advancing ship in a towing tank with floating paraffin-wax pieces acting as ice. They decomposed the resistance into two parts, a water resistance similar to an open ocean case and an ice resistance resulting from the ship-ice contact. They reported that the ice resistance can be as large as the water one, indicating the importance of accurately predicting it. Subsequently, Luo et al. (2018) conducted similar experiments but in a heading wave condition to assess the seakeeping performance of a ship in the ice floe environment; they reported the wave-ice coupling effect can increase the motion amplitude of a ship in waves.

The prohibitive cost of such experiments provides an impetus to explore the possibility of building a computational model to simulate the process. Successful modelling of ice floes has been achieved using the Discrete Element Method (DEM). A review on this has been given by Tuhkuri and Polojarvi (2018), mentioning a few works that have studied the ice-induced resistance on a ship (Lau et al., 2011; Zhan and Molyneux, 2012; Ji et al., 2013). However, these studies did not couple fluid flow directly into the process; in other words, they solved the ship-ice contact separately and added it onto a specified water resistance; such a treatment retains space for improvement. The process of a ship advancing in floating ice floes can be summarised as the following ship-wave-ice interaction: ship advancement generates waves; waves interact with ice floes; ice floes contact with the ship. The ship-generated waves can play a key role within the process; for example, it can change the velocity (magnitude and direction) of the ice floes. Therefore, ignoring the fluid flow effect may severely impact the influence of ice floes on a ship.

A more realistic computational model for the above process is in shortage, while the gap is to introduce fluid flow, including to obtain fluid field and to count its effect on ice floes. The fluid field with an advancing ship can be obtained using the Computational Fluid Dynamics method (CFD), which has been widely adopted and shown reliable accuracies (Wackers et al., 2011). On the other hand, CFD also can solve the behaviour of ice floes in waves (Huang et al., 2019; Huang and Thomas, 2019). These CFD models may be further incorporated with DEM to include potential ship-ice and ice-ice contacts, thus achieving an integrated model to simulate the current problem, which makes the goal of present work.

Therefore, this work develops an approach to incorporate DEM ice floes with a traditional CFD model of ship advancement in open ocean, by which a ship, fluid and ice floes are coupled in an all-in-one simulation. Relevant numerical theories and practicalities are introduced, followed by investigations focussing on ship resistance, as it is the most essential index for commercial shipping. The ship-wave-ice interaction at different ship-speed and ice conditions are presented, and the cause and change-rule of the resistance is analysed. Accordingly, suggestions are provided for future Arctic ship design.

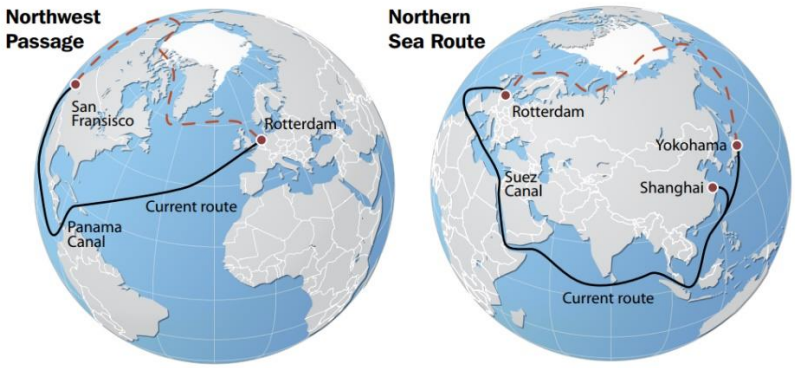

Figure 1: Comparison between traditional shipping routes (black solid line) and the Arctic shipping routes (red dash line) (Monitoring, 2012)

Figure 2. A ship advancing in pancake ice (credit to Alessandro Toffoli, University of Melbourne.)

NUMERICAL APPROACH

A numerical model is built based on the STAR-CCM+ software, including two parts: (a) a standard CFD model of ship advancing in open water, where fluid solutions are obtained; (b) DEM ice floes, which are coupled into the CFD model by a novel array-inject method, so that a continuous ice-floe region is generated for the ship to enter.

2.1 Ship Model and fluid domain

A modern container ship model, KRISO Container Ship (KCS), was adopted as the ship model for this study. KCS is a typical container ship model that has been widely applied to computational simulations, and its geometry with all of the appendages can be found in the public domain (Kim et al., 2001). The length of the hull was L_{pp} = 230 m at full scale with a scale ratio of 1:52.667 applied in this study, resulting in a model length Lpp = 4.367 m and breadth B = 0.611 m. The hull parameters are summarised in Table 1.

Following the guidelines of International Towing Tank Conference (2014), an open-ocean fluid domain was built with the recommended domain size and boundary conditions, as shown in

Figure 3. The computational domain is three-dimensional, defined by the earth-fixed Cartesian coordinate system O-*xyz*. The (*x, y*) plane is parallel to the horizon, and the *z*-axis is positively upwards. The domain size is sufficiently large to avoid the ship-generating waves being reflected from the boundaries. The lower part of the domain is filled with water and the remainder is filled with air. The hull is fixed at the free surface according to its designed draught and the ship surface is modelled as a no-slip wall. The water was initialised as flowing with a constant velocity (U_{water}) against the bow of the hull, and a constant velocity condition is applied to the inlet boundary to maintain a stable water flow entering the domain. Thus, a relative velocity exists between the ship and water, where U_{water} indicates the advancing speed of the ship in calm water. A zero-normal-gradient condition for pressure is applied to other boundaries.

The solution of the fluid domain was obtained by solving the Reynolds-averaged Navier-Stokes (RANS) equations for an incompressible Newtonian fluid:

$$\nabla \cdot \overline{\mathbf{v}} = 0 \tag{1}$$

$$\frac{\partial(\rho\overline{\mathbf{v}})}{\partial t} + \nabla \cdot (\rho\overline{\mathbf{v}}\overline{\mathbf{v}}) = -\nabla\overline{p} + \nabla \cdot \left(\overline{\tau} - \rho\overline{\mathbf{v}'\mathbf{v}'}\right) + \rho g \tag{2}$$

where $\overline{\mathbf{v}}$ is the time-averaged velocity, $\mathbf{v}'$ is the velocity fluctuations, ρ stands for the density, $\overline{p}$ denotes the time-averaged pressure, $\overline{\tau} = \mu[\nabla v + (\nabla v)^T]$ is the viscous stress term, μ is the dynamic viscosity and g is gravitational acceleration set at 9.81 m/s^2. Since the RANS equations have considered the turbulent fluid, the Shear Stress Transport (SST) k − ω model (Menter, 1993) was adopted to close the equations. The SST k − ω model has been proposed to be the most appropriate option among standard RANS turbulence models for predicting the flow field around a ship hull (Zhang et al., 2006).

The free surface between the air and water was modelled by the Volume of Fluid (VOF) method (Hirt and Nichols, 1981). The VOF method introduces a passive scalar α, denoting the fractional volume of a cell occupied by a specific phase. In this case, a value of α = 1 corresponds to a cell full of water and a value of α = 0 indicates a cell full of air. Thus, the free surface, which is a mix of these two phases, is formed by the cells with $0 < \alpha < 1$. The elevation of the free surface along time is obtained by the advection equation of α, expressed as Equation (3). For a cell containing both air and water, its density and viscosity are determined by a linear average according to Equation (4) and Equation (5). In this study, ρ_{water} = 998.8 kg/m^3, μ_{water} = 8.90×10^{-4} N·s/m^2; ρ_{air} = 1 kg/m^3, μ_{air} = 1.48×10^{-5} N·s/m^2. The governing equations of the fluid domain were discretised and solved using the Finite Volume method (Versteeg and Malalasekera, 2007).

$$\frac{\partial\alpha}{\partial t} + \nabla \cdot (\overline{\mathbf{v}}\alpha) = 0 \tag{3}$$

$$\rho = \alpha\rho_{water} + (1-\alpha)\rho_{air} \tag{4}$$

$$\mu = \alpha\mu_{water} + (1-\alpha)\mu_{air} \tag{5}$$

Table 1. Main dimensions of the KCS hull.

	Model scale	Full scale
Length between perpendiculars (m)	4.367	230.0
Waterline breadth (m)	0.611	32.2
Draught midships (m)	0.205	10.8
Trim angle (rad)	0.0	0.0
Block coefficient (-)	0.651	0.651
Wetted surface (m^2)	3.435	8992.0

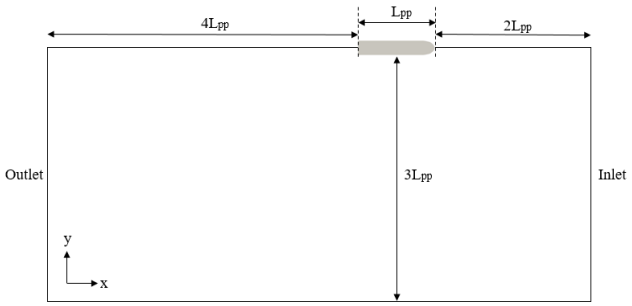

(a) plan view; only half of the domain is shown but no symmetry plane condition is applied.

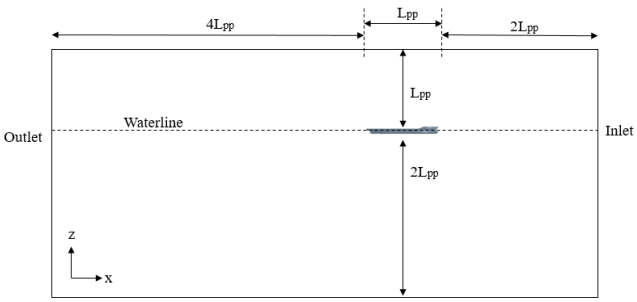

(b) profile view.

Figure 3. Illustration of the computational domain with dimensions.

2.2 Ice floe Modelling

The simulation first runs for a certain time without sea ice to allow the fluid domain to achieve a steady-state, i.e. when the ship-generated waves become stable. Subsequently, an array of pancake ice floes is injected near the inlet of the fluid domain, as shown in Figure 4(a). Each ice floe array is set as six rows combined with enough columns that cover a width affecting the ship, in which, the distance between the centres of two ice floes is set to be equal (d = d1 = d2). Every second row is in a position interval of the previous one and it repeats. The ice floes are initialised as floating on the water surface according to their buoyancy-gravity equilibrium position and at the same velocity as the water flow ($U_{ice} = U_{water}$). One ice floe array is injected to the same region every $t_{inject} = 6d/U_{ice}$, so that the next ice floe array can just follow the former one with the same distribution, as shown in Figure 4(b). Thus, the injection of ice floes does not influence the stability of the fluid domain around the ship and the ship can enter a

continuous ice-floe area, as desired, shown in Figure 5. With this method, an ice-floe route of any desired length can be achieved with a minimal domain size, which can significantly reduce the computational costs. By contrast, in previous studies, all ice floes are injected at once for a ship to go through, which requires a very long domain.

Following the nature of pancake ice, each ice floe is modelled as a rigid thin disk, with its thickness h = 0.02 m, density ρ_{ice} = 900 kg/m^3, and diameter D, which will be varied to study its influence. Another important parameter to be investigated is the concentration of the ice floes (C), which indicates the percentage of the water surface covered by sea ice:

$$C = \frac{\pi \times (0.5D)^2}{d^2} \times 100\% \tag{6}$$

The ice floes are modelled as DEM particles in the Lagrangian framework moving in the Eulerian fluid domain (Baran, 2012). The movement of an ice floe can be considered as the combination of translation and rotation, which was solved with the rigid-body motion equations in the body-fixed system based on the mass centre of the floe G–$x'y'z'$:

$$\mathbf{F} = m\frac{d\overrightarrow{V_G}}{dt} \tag{7}$$

$$\mathbf{T} = [\mathrm{J}] \cdot \frac{d\overrightarrow{\omega_G}}{dt} + \overrightarrow{\omega_G} \times ([J] \cdot \overrightarrow{\omega_G}) \tag{8}$$

where **F** and **T** are the total force and torque on the ice floe, induced by the gravity, the hydraulic load from surrounding fluid $\boldsymbol{F_h}$ and contact force **Fc** from ship-ice contact or ice-ice contact; m and [J] are the mass and inertia moment tensor respectively, and V_G and ω_G are the translational and rotational velocity vectors of the ice floe.

The hydraulic force $\mathbf{F_h}$ can be calculated based on the solution from the fluid domain, as expressed in Equation (9). The fluid solution and ice floes are linked based on a one-way coupling, i.e. the ice movement does not provide feedback to the fluid domain. A two-way coupling has also been tested, while the ship resistance did not show a clear change, therefore, a two-way method is deemed to be unnecessary since it would bring about a significant increase in computational load.

$$\boldsymbol{F_h} = \int (-\overline{p}\,\boldsymbol{n} + \overline{\tau} \cdot \boldsymbol{n})\, dS \tag{9}$$

The contact force **Fc** is calculated by a penalty method (Cundall and Strack, 1979), where ship/ice and ice/ice are allowed to have an overlap, according to the movement solution. The overlap is modelled as a linear spring-dashpot system where the spring (k) accounts for the elastic response and the dashpot (η) reflects the energy dissipation during the contact, by which the normal and tangential components of **Fc** are calculated according to Equation (10) and (11) respectively. Subsequently, the contact force pushes the overlapped bodies apart so that the overlap is minimised in the final solution.

$$\mathbf{F_n} = -kd_n - \eta v_n \tag{10}$$

$$\mathbf{F_t} = \begin{cases} -kd_t - \eta v_t\,, & if\ |d_t| < |d_n|\mathrm{C}_f \\ |kd_n|\mathrm{C}_f \cdot \boldsymbol{n}\,, & if\ |d_t| \geq |d_n|\mathrm{C}_f \end{cases} \tag{11}$$

where d_n and d_t are overlap distances in the normal and tangential directions respectively, v_n and v_t are the normal and tangential components of the relative velocity between two contact bodies, $\mathrm{C_f}$ is the friction coefficient of sea ice, set at 0.35; k was set at 10^4 N/m and $\eta = 2C_{damp}\sqrt{kM_{eq}}$, in which C_{damp} was set at 0.067 and M_{eq} is the equivalent mass of two contact bodies, calculated as $M_{eq} = M_A M_B/(M_A + M_B)$.

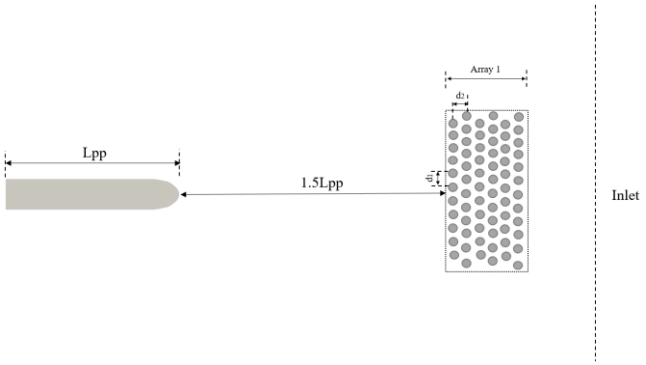

(a) t = t_1 when the first ice array is injected

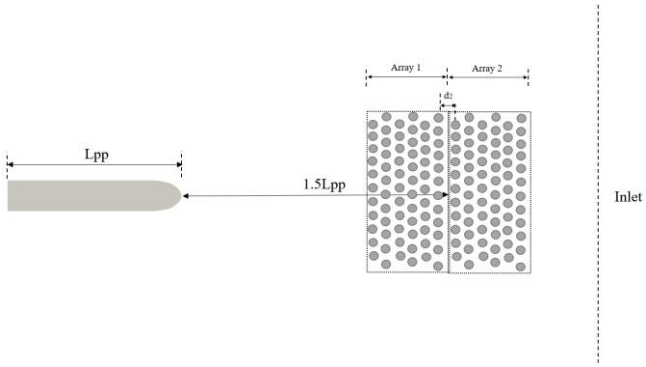

(b) t = t_1 + t_{inject} when the second ice array is injected

Figure 4. Illustration of how ice floes are added to the CFD model

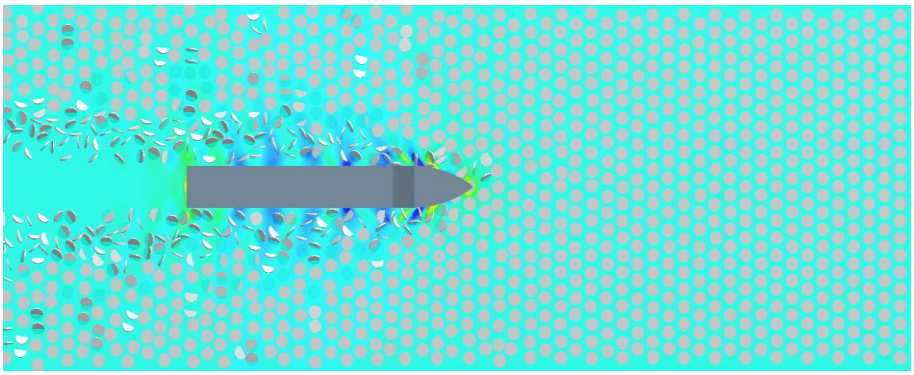

Figure 5. A ship advancing in an ice-floe region

RESULTS AND DISCUSSION

As shown in Figure 6, when the ship is advancing in the ice floe region, ship-ice collisions occur at the bow area, causing the floes to be pushed aside and rotate within the wake, and in some cases, floes can slide along the ship before being pushed away. This study focuses on analysing the ship resistance, which consists of an ice resistance R_{ice} induced by the floes and a water resistance R_{water} similar to an open-ocean case ($R_{total} = R_{ice} + R_{water}$), in which, R_{ice} is due to ship-ice collisions at the bow area and friction caused by the floes sliding along the ship.

The proposed model was first validated against the experiments conducted at the towing tank of Harbin Engineering University (Guo et al. 2018). The computational settings follow an accordant manner with the experiment, and comparisons were conducted for ship speed from 0.4 m/s to 1.2 m/s, corresponding to Froude number Fr = 0.06 - 0.18. The comparison between computational and experimental results is shown in Figure 7, where good agreement can be seen for all the examined speeds, showing a good accuracy of the model in predicting ship resistance in pancake ice. Figure 7 also contains the open water component, and R_{ice} can be seen as the difference between the two curves. The resistance curves with and without ice both show an exponential increase with increasing speed, while the changing of R_{ice} has a lower power than that of R_{water}.

Subsequently, ship speed, ice concentration and floe diameter were varied to investigate their influences on the resistance. Figure 8 presents the resistance as a function of Fr, C and D/B (floe diameter divided by ship breath). A horizontal comparison between Figure 8(a), (b) and (c) demonstrates R_{total}/R_{water} is larger in at a lower velocity condition, which means R_{ice} is more influential when the ship is relatively slow. The difference is because a faster ship generates stronger waves, which pushes the floes away thus reducing the collision and friction. This also confirms the great importance of the inclusion of fluid flow in present work.

The influence of ice concentration and floe diameter on the resistance were further analysed by holding one constant and varying the other. Figure 9(a) presents the ship resistance for the same floe size but different ice concentrations, in which it is clear that denser ice brings a higher resistance to the ship. This results from a higher frequency of collision and more ice floes sliding along the ship. Figure 9(b) compares the ship resistance for the same ice concentration but different floe diameters. Although a larger floe size leads to sparser ice and also lowers the collision frequency, the resistance shows an obvious increase. The increase mainly comes from the higher collision force induced by larger floes, whose effect on ship resistance proves to be more dominant than a lower collision frequency. As a result, the overall force integration over time still increases. In an overall view, both C and D show a quasi-linear relationship with the resistance, which suggests empirical equations may be further derived for a more convenient prediction of ship resistance in pancake ice. This would be of use for future Arctic optimisation tools to provide a power estimate of different routes.

In practice, the concentration and diameter data can be taken from actual Arctic shipping routes and inputted into the simulation, so as to suggest the extra-required power relative to an open-ocean case. Such ice data can be obtained from field measurements and aerial observations (Parmiggiani et al., 2018; Thomson et al., 2018), even appropriate predictions. In addition, the simulation shows the collision force contributes much more to ice resistance than the friction does. Therefore, future Arctic ship design may give primary consideration to designing devices to reduce the collisions at the bow area. For example, a device can be installed at the bow to jet water, so that ice floes can be pushed away before colliding with the ship. For a secondary consideration of reducing the friction, certain surface treatments may be applied to make the ship smoother. Otherwise, with a large proportion of ice-added resistance in the ship resistance, the advantage of shorter Arctic shipping routes will not necessarily mean a significant energy saving to be achieved.

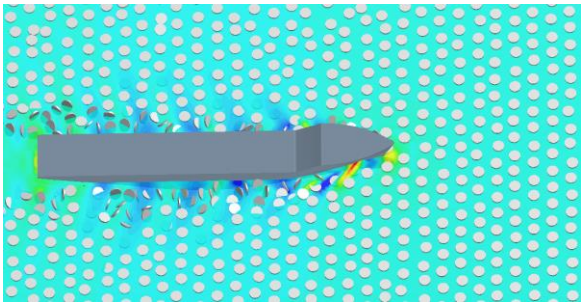

(a) C = 30% and D = 0.15 m

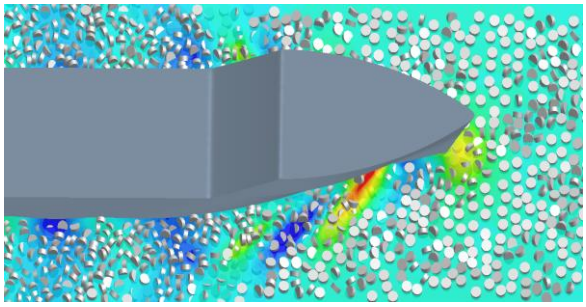

(b) C = 50% and D = 0.05 m

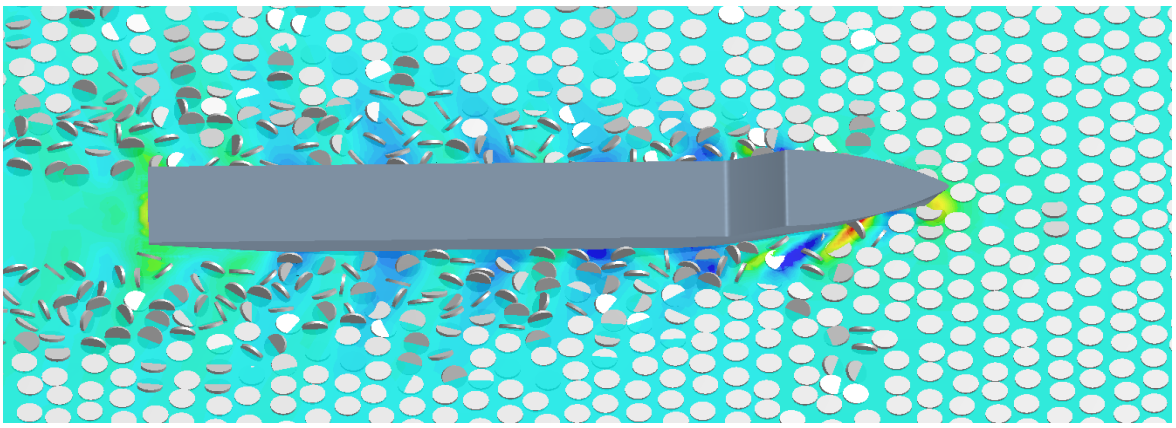

(c) C = 50% and D = 0.15 m

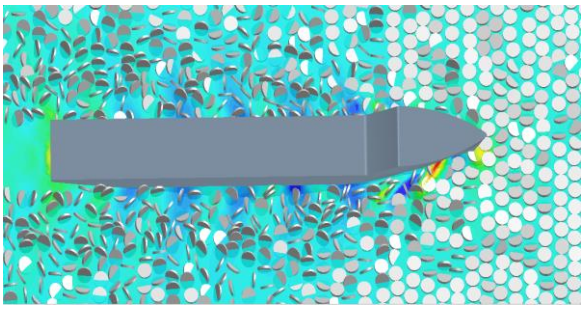

(d) C = 70% and D = 0.15 m

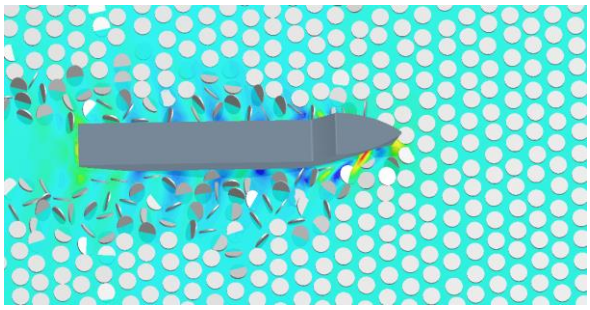

(e) C = 50% and D = 0.25 m

Figure 6. Close-up of the ship-wave-ice interaction in different ice conditions

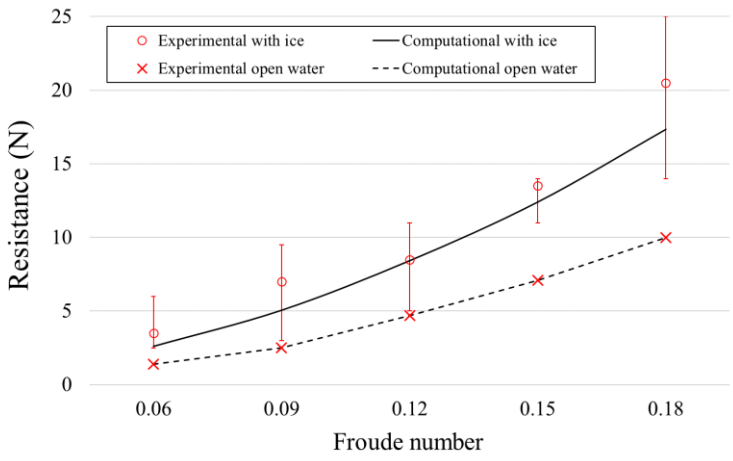

Figure 7. Experimental (Guo et al. 2018) and computational resistance in pancake ice, when C = 60% and D/B = 0.57, attended by open-water counterpart.

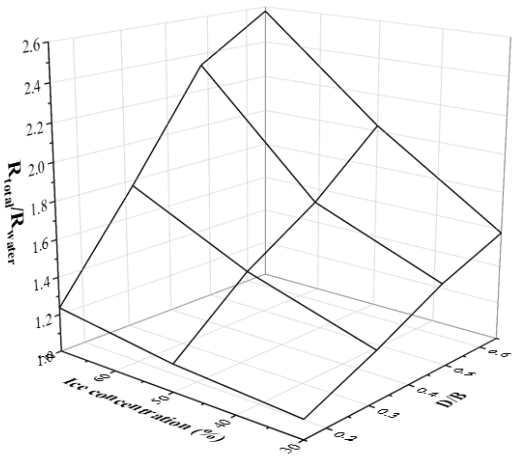

(a) Fr = 0.06

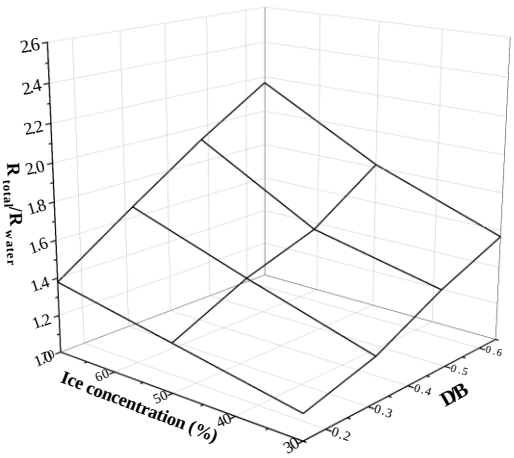

(b) Fr = 0.12

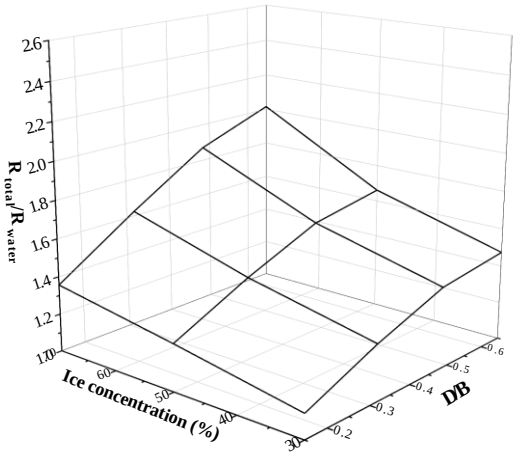

(c) Fr = 0.18

Figure 8. Total ship resistance normalised by open water counterpart, at different ship speeds, ice concentrations and floe diameters

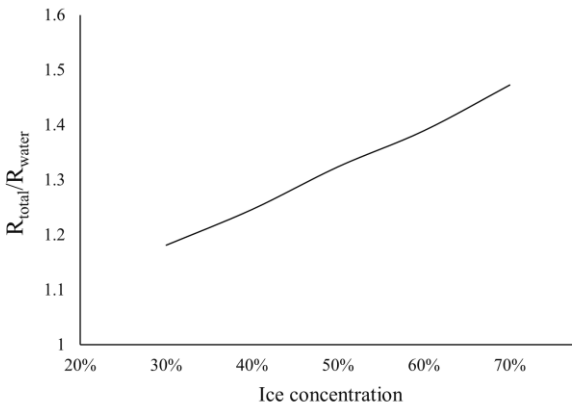

(a) D/B = 0.25 m with varying C

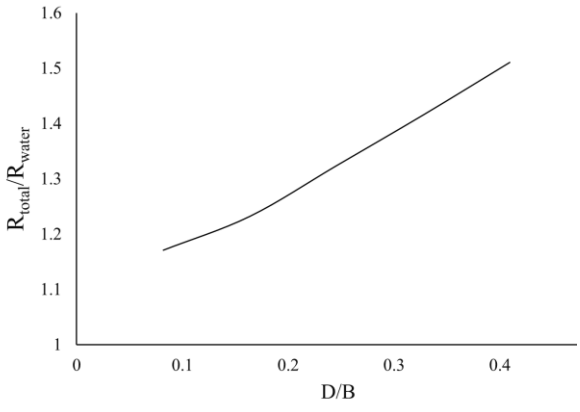

(b) C = 50% with varying D

Figure 9. Influence of ice concentration and floe diameter on total resistance, when Fr = 0.15.

CONCLUSIONS

A computational model has been developed to predict the performance of a ship advancing in pancake ice, since such a condition has been reported to be the main navigation environment of future Arctic. Relevant numerical theories and practicalities have been introduced in detail, by which DEM ice floes are incorporated with a traditional CFD model so that a ship advancing in continuous ice floes has been achieved with a minimal domain size. After validated against experiments, the proposed model has shown to be capable of accurately predicting the ship resistance.

Extended investigations have shown that ice floes can be a significant part in the total ship resistance, and it is highly dictated by ship speed, ice concentration and floe size. This work is the first model that includes fluid flow to simulate the whole ship-wave-ice interaction process, which proves to be of great importance: the ship-generated waves have been demonstrated to reduce the ice resistance, and it leads to the finding that ice-added resistance is more influential when the ship is relatively slow. In addition, both ice concentration and floe size have shown a quasi-linear relationship with the resistance.

The proposed model has the potential to be a practical tool providing valuable insights for Arctic shipping, and the nature of simulation makes it convenient and cost-effective. It may serve for (1) power estimate: calculate ship-power according to resistance prediction. (2) material design: based on the collision frequency and force to assess material fatigue, as well as selecting appropriate materials and determining structural scantlings. (3) hull optimisation: compare different hull designs and suggest the suitability in a given ice condition (4) stability and safety: predict ship motions and generate ocean waves to study the seakeeping performance.

ACKNOWLEDGEMENTS

This work is part of a project that has received funding from the European Union's Horizon 2020 research and innovation programme under grant agreement No 723526 - SEDNA: Safe maritime operations under extreme conditions; the Arctic case. The authors are grateful to the High-Performance Computing service provided by University College London (UCL) and the associated support from the IT team and Mr Andrea GL Rosa.

REFERENCES

Baran, O., 2012. Discrete element method in STAR CCM+, in: STAR Japanese Conference.

Cundall, P.A., Strack, O.D., 1979. A discrete numerical model for granular assemblies. geotechnique 29, 47–65.

Guo, C., Xie, C., Zhang, J., Wang, S., Zhao, D., 2018. Experimental Investigation of the Resistance Performance and Heave and Pitch Motions of Ice-Going Container Ship Under Pack Ice Conditions. China Ocean Eng 32, 169–178. https://doi.org/10.1007/s13344-018-0018-9

Hirt, C.W., Nichols, B.D., 1981. Volume of fluid (VOF) method for the dynamics of free boundaries. Journal of computational physics 39, 201–225.

Huang, L., Ren, K., Li, M., Tukovic, Z., Cardiff, P., Thomas, G., 2019. Fluid-structure interaction of a large ice sheet in waves. Ocean Engineering.

Huang, L., Thomas, G., 2019. Simulation of Wave Interaction With a Circular Ice Floe. Journal of Offshore Mechanics and Arctic Engineering 141, 041302.

ITTC, 2014. Guidelines: Practical Guidelines for Ship CFD Applications. ITTC Report 7–5.

Ji, S., Li, Z., Li, C., Shang, J., 2013. Discrete element modeling of ice loads on ship hulls in broken ice fields. Acta Oceanologica Sinica 32, 50–58.

Kim, W.J., Van, S.H., Kim, D.H., 2001. Measurement of flows around modern commercial ship

models. Experiments in fluids 31, 567–578.
Lau, M., Lawrence, K.P., Rothenburg, L., 2011. Discrete element analysis of ice loads on ships and structures. Ships and Offshore Structures 6, 211–221.
Luo, W.-Z., Guo, C.-Y., Wu, T.-C., Su, Y.-M., 2018. Experimental research on resistance and motion attitude variation of ship–wave–ice interaction in marginal ice zones. Marine Structures 58, 399–415. https://doi.org/10.1016/j.marstruc.2017.12.013
Menter, F., 1993. Zonal two equation kw turbulence models for aerodynamic flows, in: 23rd Fluid Dynamics, Plasmadynamics, and Lasers Conference. p. 2906.
Monitoring, A., 2012. Changes in arctic snow, water, ice and permafrost. swipa 2011 overview report. Arctic Climate.
Ørts Hansen, C., Grønsedt, P., Lindstrøm Graversen, C., Hendriksen, C., 2016. Arctic shipping–commercial opportunities and challenges. Copenhagen Business School Maritime.
Parmiggiani, F., Moctezuma-Flores, M., Wadhams, P., Aulicino, G., 2018. Image processing for pancake ice detection and size distribution computation. International Journal of Remote Sensing 1–16.
Smith, L.C., Stephenson, S.R., 2013. New Trans-Arctic shipping routes navigable by midcentury, in: Proceedings of the National Academy of Sciences. pp. E1191–E1195.
Stroeve, J.C., Kattsov, V., Barrett, A., Serreze, M., Pavlova, T., Holland, M., Meier, W.N., 2012. Trends in Arctic sea ice extent from CMIP5, CMIP3 and observations. Geophysical Research Letters 39. https://doi.org/10.1029/2012GL052676
Thomson, J., Ackley, S., Girard-Ardhuin, F., Ardhuin, F., Babanin, A., Boutin, G., Brozena, J., Cheng, S., Collins, C., Doble, M., 2018. Overview of the arctic sea state and boundary layer physics program. Journal of Geophysical Research: Oceans.
Tuhkuri, J., Polojärvi, A., 2018. A review of discrete element simulation of ice–structure interaction. Philosophical transactions. Series A, Mathematical, physical, and engineering sciences 376.
Versteeg, H.K., Malalasekera, W., 2007. An introduction to computational fluid dynamics: the finite volume method. Pearson Education.
Wackers, J., Koren, B., Raven, H.C., Van der Ploeg, A., Starke, A.R., Deng, G.B., Queutey, P., Visonneau, M., Hino, T., Ohashi, K., 2011. Free-surface viscous flow solution methods for ship hydrodynamics. Archives of Computational Methods in Engineering 18, 1–41.
Zhan, D., Molyneux, D., 2012. 3-Dimensional Numerical Simulation of Ship Motion in Pack Ice, in: ASME 2012 31st International Conference on Ocean, Offshore and Arctic Engineering. American Society of Mechanical Engineers, pp. 407–414.
Zhang, Z., Liu, H., Zhu, S., Zhao, F., 2006. Application of CFD in ship engineering design practice and ship hydrodynamics. Journal of Hydrodynamics 18, 308–315.